Time-Delay Margin and Robustness of Incremental Nonlinear Dynamic Inversion Control

Huang, Y.; Zhang, Ye; Pool, D.M.; Stroosma, O.; Chu, Q. P.

Important note
To cite this publication, please use the final published version (if applicable).
Please check the document version above.

Time-Delay Margin and Robustness of Incremental Nonlinear Dynamic Inversion Control

Yingzhi Huang *, Ye Zhang[†]
Northwestern Polytechnical University, Xi'an, China.

Daan M. Pool[‡], Olaf Stroosma[§] , and Qiping Chu[¶]
Delft University of Technology, Delft, The Netherlands.

I. Introduction

Nonlinear Dynamic Inversion (NDI) is a nonlinear feedback linearization technique that has been widely applied to flight control systems [1, 2]. Using state feedback and the inverted nonlinear system dynamics, NDI can significantly reduce controller development costs by avoiding gain scheduling and Jacobian linearization at a multitude of operating points. However, the control performance of NDI is directly dependent on required detailed knowledge of the model. As a simplified and enhanced NDI method [3], Incremental Nonlinear Dynamic Inversion (INDI) [4, 5] has been proposed to reduce the model dependency and improve the robustness against model uncertainties. Instead of using a global nonlinear model, in INDI the dynamic inversion is implemented on a locally linearized system model that is updated at every sampling period, for which the control input is calculated in an incremental manner. Unlike NDI, for which full knowledge of the complete system dynamics is needed, INDI only requires explicit knowledge of the system's control effectiveness matrix.

Due to its robustness against model uncertainties and improved performance compared to NDI, there has been a rapid development in INDI's implementation in various practical flight control applications, including Micro Air Vehicles (MAVs) [6, 7], helicopters [8] and fixed-wing passenger aircraft [9]. Despite its practical success, however, some essential theoretical problems regarding INDI's stability and robustness were still left unsolved. In addition to INDI, other similar control strategies based on incremental control have been proposed, i.e., Time-Delay Control (TDC) [10], Model-Free Adaptive Control (MFAC) [11], Incremental Backstepping (IBKS) [12, 13], Incremental Sliding Mode Control (ISMC) [14] and Incremental Approximate Dynamic Programming [15]. The common feature of these control methods is the combination of an incremental dynamic model under a high sampling rate with their corresponding baseline nonlinear controllers. However, as is also the case for INDI, in general the corresponding time-delay margins and robustness tolerances against parameter uncertainties, especially when considering actuator dynamics, are not explicitly quantified.

---

*Associate Professor, School of Power and Energy; huangyingzhi@nwpu.edu.cn. Member AIAA

[†]Associate Professor, School of Astronautics; zhang_ye@nwpu.edu.cn (corresponding author). Member AIAA

[‡]Assistant Professor, Control and Simulation Section, Faculty of Aerospace Engineering; d.m.pool@tudelft.nl. Senior Member AIAA

[§]Senior Researcher, Control and Simulation Section, Faculty of Aerospace Engineering; o.stroosma@tudelft.nl. Senior Member AIAA

[¶]Associate Professor, Control and Simulation Section, Faculty of Aerospace Engineering; q.chu@tudelft.nl. Member AIAA

Therefore, this Note aims to address these open theoretical problems regarding the robustness of incremental methods. First, there is a lack of stability condition analysis in terms of the controller sampling rate. The current design and stability analysis of incremental methods assume a sufficiently high sampling rate of the controller, which means that given a particular controller sampling rate, one cannot guarantee the stability or determine the stability margin of the control system. In a few recent studies on the stability analysis of INDI, the stability condition is given either with a sufficient condition under an infinitely high sampling rate for the controller[16], or for a case study with a specific (high) controller sampling rate [17]. None of these studies came up with a quantified limit for the lowest stable sampling frequency, so the current INDI control law design can only depend on a rule of thumb. Second, in the presence of model uncertainties in the control effectiveness matrix, the robustness and stability of INDI is still an open question. In various simulation and real-world tests INDI is shown to be robust, even with parameter mismatches up to 50% [4, 5, 9]. However, no systematic theory exists in literature that explains these results and calculates a quantified stability condition regarding control effectiveness uncertainties, i.e., the maximum level of model mismatch for which an INDI-controlled system remains stable. Third, the basic INDI theory is derived under the assumption of infinitely fast actuators, which do not exist in reality. No available theoretical analysis addresses how the stability and robustness of INDI-controlled systems will be influenced by realistic actuator dynamics.

This Note addresses the aforementioned theoretical problems of the INDI control method. As the finite sampling period of INDI controller inherently introduces (identical) time delays in the feedback of state derivatives and the control inputs [4, 5, 8], the stability condition with respect to the controller sampling rate can be derived from the time-delay margin of the controlled system. It will be shown that in existence of model uncertainty in the control effectiveness matrix, INDI intentionally turns the original system dynamics without time delay into a special class of Neutral Functional Differential Equations (NFDE) [18] with a time delay and a unique parameter structure. Based on the equivalent NFDE system, the time-delay margin of the INDI-controlled system can be determined and its tolerance to the control effectiveness uncertainties can be quantified, together with a stability condition. Furthermore, by taking actuator dynamics into account, it will be proven that the controlled system dynamics are turned into high-order Retarded Functional Differential Equations (RFDE) [18] and the corresponding stability condition in terms of the time-delay margin and the tolerance to control effectiveness uncertainties can be analytically derived. Note that in this Note we use the largest deviation of model parameter from its true value that maintains a stable control system to measure how much stability margin exists under model mismatches. We call this largest tolerable deviation the "*parameter uncertainty bound*", in order to distinguish it from the classic stability margin definition. To the best of the authors' knowledge, this is the first quantified theoretical analysis of the time-delay margin and robustness for the INDI method that explicitly addresses control effectiveness uncertainties and practical actuator dynamics. Thus, for practitioners, this Note also serves as a guideline for choosing optimal sampling rates and control effectiveness parameters when designing INDI controllers. The derived stability condition with respect to control effectiveness

uncertainties and time delay is validated by simulations of a fully nonlinear model of a fixed-wing aircraft.

II. Incremental Nonlinear Dynamic Inversion

Nonlinear Dynamic Inversion (NDI) can be applied to nonlinear systems that are feedback linearizable [19] with good knowledge of the model. In order to reduce the model dependency, the INDI technique transforms the nonlinear system dynamics into an incremental form, in which the model dependency can be minimized, before implementing the dynamic inversion. The INDI control method is briefly reviewed as follows.

Consider a general control inputs affine system given by

$$\dot{x} = f(x) + G(x) u$$
$$y = h(x)$$
(1)

where $x \in \mathbb{R}^n$ is the state vector, $u \in \mathbb{R}^m$ is the input vector, $y \in \mathbb{R}^p$ is the output vector, $f : \mathbb{R}^n \to \mathbb{R}^n$, $h : \mathbb{R}^n \to \mathbb{R}^p$ are smooth vector fields and $G : \mathbb{R}^n \to \mathbb{R}^{n \times m}$ is a smooth function. x, f, G and h are assumed to be continuous. If $p < m$ or $p > m$, the input-output linearization of Eq. (1) becomes an over-determined or under-determined control problem. In this Note $p = m$ is assumed for the following derivations.

The standard procedure of feedback linearization for the general system of Eq. (1) requires the consecutive differentiation of each channel of y until each element of the input u explicitly shows up [20]. The vector of required differentiation numbers are defined as the relative degree of the system, i.e., $r = (r_1, r_2, ..., r_m)$, and the total relative degree r_d is the sum over the relative degree of each output, i.e., $r_d = \sum_{i=1}^{m} r_i$. The system is full-state linearizable if the total relative degree $r_d = n$ [19]. If $r_d < n$, the system has $n - r_d$ degrees of internal dynamics, the stability of which determines the stability of the total feedback-linearized system.

For simplicity, assume that $h(x) = x$, the relative degree of the system is $(1, \ldots, 1)_{1 \times n}$ and no internal dynamics exist. In this case, the control input u appears explicitly by taking the first-order derivative of the output:

$$\dot{y} = \dot{x} = f(x) + G(x) u$$
(2)

Before implementing a direct dynamic inversion, the INDI method considers a first-order Taylor series expansion of Eq. (2) around the beginning instant of each sampling interval (denoted by subscript 0):

$$\dot{x} \approx \dot{x}_0 + G(x_0)(u - u_0) + \frac{\partial [f(x) + G(x) u]}{\partial x}\bigg|_0 (x - x_0) + O\left[(x - x_0)^2\right]$$
(3)

in which the system derivative $\dot{x}_0$ at each sampling instant is assumed to be available from sensor measurements. Neglecting the higher order terms, Eq. (3) essentially means that at each sampling period, the nonlinear system Eq. (2) is estimated with a local linear system with Jacobian linearization:

$$\dot{x} = Fx + Gu$$
(4)

3

where

$$F = \frac{\partial \left[f\left(x \right) + G\left(x \right) u \right]}{\partial x} \bigg|_0 , \ G = G\left(x_0 \right) \tag{5}$$

Note that due to this linearization, Eqs. (3) and (4) are only valid within a small region around $\dot{x}_0$. If we measure $\dot{x}\left(t \right)$ and update it at the beginning of every sample point, and always consider the Taylor approximation within only one sample, a high measurement sampling rate will in general directly ensure that this requirement is satisfied. In this way we avoid the disadvantage of using a traditional fixed point for the Taylor series approximation. With this feature and the assumption of sufficiently high measurement sampling rate, F and G can be considered to be constants or slowly varying parameters within many samples. This allows for using linear system theory for the derivation of the quantified stability criterion. The simulation results using a fully nonlinear model given in this Note provide direct verification of the accuracy of the derived stability condition.

The INDI control law is obtained from Eq. (3). Considering the continuity of system state x, taking the limit of both sides of Eq. (3) as the time step τ approaches zero we obtain:

$$\dot{x} = \lim_{\tau \to 0} \dot{x} = \lim_{\tau \to 0} \dot{x}_0 + \frac{\partial}{\partial x} \left[f\left(x \right) + G\left(x \right) u \right]_{x_0, u_0} \lim_{\tau \to 0} \left(x - x_0 \right) + G\left(x_0 \right) \lim_{\tau \to 0} \left(u - u_0 \right)$$

$$= \dot{x}_0 + G\left(x_0 \right) \left(u - u_0 \right) \tag{6}$$

where the control input u and state derivative $\dot{x}$ are not necessarily continuous. Assume that G is invertible, the INDI control law is obtained by performing the dynamic inversion on Eq. (6):

$$u = u_0 + \hat{G}^{-1} \left(v - \dot{x}_0 \right) \tag{7}$$

where $\dot{x}_0$ and u_0 are the measured or estimated system state derivative and input command at the most recent controller sample respectively, $\hat{G}$ is the estimation of its real value, and $v \in \mathbb{R}^m$ is called the pseudo-control input. If the estimated control effectiveness matrix $\hat{G}\left(x \right)$ is identical to its real value, the controlled system is turned into a perfect single integrator

$$\dot{x} = v \tag{8}$$

and a simple linear controller can be easily chosen to generate v for stabilizing or tracking missions for x.

In practice, the INDI controller is essentially discrete and updated at every time sample. Denoting the controller sampling time by τ, the implementable control law of Eq. (7) can be written in a more explicit form:

$$u\left(t \right) = u\left(t - \tau \right) + \hat{G}^{-1} \left[v\left(t \right) - \dot{x}\left(t - \tau \right) \right] \tag{9}$$

The block diagram of the practical INDI control law of Eq. (9) is illustrated in Fig. 1, with the local linear system given by Eq. (4). It is clear from Eq. (9) that at every sampling point, only the control increment $\Delta u\left(t \right) = \hat{G}^{-1} \left[v\left(t \right) - \dot{x}\left(t - \tau \right) \right]$ is calculated and added to the delayed control input. In Fig. 1, $A\left(s \right)$ denotes the diagonal matrix
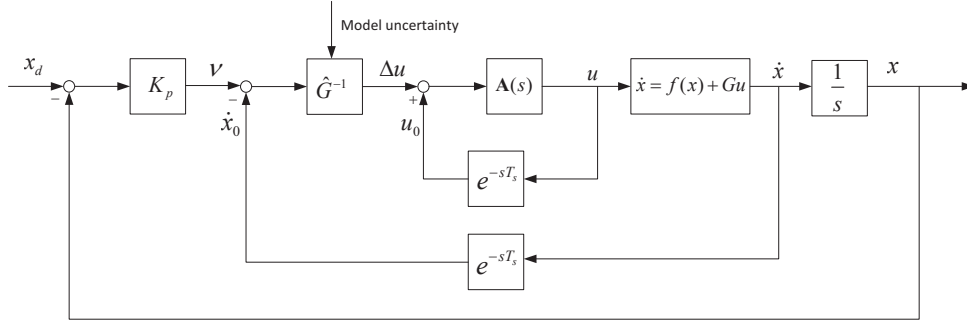
Fig. 1 General structure of an INDI controlled system ($A\,(s) = \mathbf{diag}\,(A_1\,(s)\,, A_2\,(s)\,, ..., A_n\,(s))$)

of the n actuator dynamics, i.e., $A\,(s) = \mathrm{diag}\,(A_1\,(s)\,, A_2\,(s)\,, ..., A_n\,(s))$.

By explicitly describing the sampling time as a time delay τ in Eq. (9), the stability condition for the sampling frequency is transformed into the task of calculating the *time-delay margin* of the resulting controlled system. As will also be derived in the next section, the explicit discussion of the time delay reveals, for the first time, that any uncertainties in $\hat{G}\,(x)$ for INDI introduce additional time-delay dynamics to the single integrator of Eq. (8). Moreover, the stability and performance of these addition dynamics depend on the quantified model mismatch level in the control effectiveness matrix $\hat{G}\,(x)$, the time delay τ, and the bandwidth of the actuator dynamics.

III. Time-delay margin and robustness of INDI

Time-delay systems are systems with significant time lags in their dynamics. Such lags inherently exist in many practical processes in biology, chemistry, economics and various other system dynamics [21]. In this section, the INDI controlled systems are reformulated into a special class of time-delay systems with good robustness to uncertainties, and a stability condition can be determined by computing the systems' *time-delay margin*, i.e., the non-negative delay interval for which the considered system is still stable for all delay values.

A. Reformulating the INDI controlled systems

Applying the sample time τ of the INDI controller to Eq. (3), while neglecting the higher-order term, yields:

$$\dot{x}\,(t) = \dot{x}\,(t - \tau) + G\,[u\,(t) - u\,(t - \tau)] + F\,[x\,(t) - x\,(t - \tau)] \tag{10}$$

in which F and G are considered as constants or slowly varying parameters within many samples. Substituting the INDI control law in Eq. (9) into Eq. (10) we obtain

$$\overbrace{\hat{G}G^{-1}\dot{x}\,(t) + \left[I - \hat{G}G^{-1}\right]\dot{x}\,(t - \tau)}^{\text{neutral part}} - \hat{G}G^{-1}F\,[x\,(t) - x\,(t - \tau)] = v\,(t) \tag{11}$$

5

When uncertainties exist in $\hat{G}$, $I \neq \hat{G}G^{-1}$, and the system dynamics in Eq. (11) represent a typical NFDE with a single (and by definition commensurate) delay [22], as the highest order derivative contains the delay. Taking the Laplace transform of Eq. (11) while assuming all initial conditions as zero, we obtain

$$X(s) = \left(\hat{G}G^{-1}s + \left(I - \hat{G}G^{-1}\right) se^{-\tau s} - \hat{G}G^{-1}F \left(1 - e^{-\tau s}\right) \right)^{-1} \mathcal{V}(s) \tag{12}$$

based on which we can define the *characteristic quasi-polynomial* [21, 22] $p(s, e^{-\tau s})$ of the system in Eq. (11):

$$p(s, e^{-\tau s}) = \det \left(\hat{G}G^{-1}s + \left(I - \hat{G}G^{-1}\right) se^{-\tau s} - \hat{G}G^{-1}F \left(1 - e^{-\tau s}\right) \right), \quad \tau \geq 0 \tag{13}$$

The poles of the system in Eq. (11) are defined by the roots of the characteristic equations $p(s, e^{-\tau s}) = 0$. For neutral time-delay systems given in Eq. (11), before directly investigating the locations of the poles, a necessary condition for stability is that the neutral part of the system dynamics is stable [21, 23]. This requires that the following neutral part of Eq. (11) is stable:

$$\hat{G}G^{-1}\dot{x}(t) + \left[I - \hat{G}G^{-1}\right] \dot{x}(t - \tau) = 0 \tag{14}$$

The sufficient and necessary condition for the stability of Eq. (14) will be given in the proof of Proposition 2 later in this Note. Specifically for a SISO system where G is a scalar, the condition for stability is simply $\hat{G}G^{-1} > 0.5$, which is also discussed in the proof of Proposition 1. Note that we introduce Eq. (14) only for calculating its stability condition, but do not assume the equation itself to hold.

If the stability condition for Eq. (14) is met, it is guaranteed that the number of unstable roots of $p(s, e^{-\tau s}) = 0$ is finite [21, 24]. Thus, the stability condition for Eq. (11) is that none of its poles are located in the closed right-half plane. With this condition satisfied, the time-delay margin for stability is defined by [22, 23]

$$\tau^* := \inf\{\tau \ : \ p(s, e^{-\tau s}) = 0 \text{ for some } s \in \overline{\mathbb{C}}_+\} \tag{15}$$

where $\overline{\mathbb{C}}_+$ denotes the closed right-half plane. Hence, by definition, τ^* is the largest delay value for which the system remains stable, which thus defines the lower limit for the sampling frequency of an INDI controller.

The calculation of the time-delay margin for stability has been a challenging, but well-studied, topic for time-delay systems and a few survey papers provide comprehensive reviews of recent progress [21, 22]. This Note does not focus on general algorithms for general time-delay systems, but aims to reveal how the INDI controller voluntarily introduces robust time-delay dynamics between the virtual control and the controlled state with a certain time-delay margin, in the form of Eq. (12). In this section, a single-input-single-output(SISO) case will first be discussed before the obtained

result is generalized to Multiple-Input-Multiple-Output (MIMO) systems.

B. Single-Input-Single-Output (SISO) Systems

Consider a SISO system for Eq. (2), where G and F are scalars in Eq. (12). Defining $\lambda = \hat{G}G^{-1}$, which indicates the model mismatch level, and $\beta = F$, Eq. (12) can be written as:

$$\frac{sX(s)}{\mathcal{V}(s)} = H(s) = \frac{s}{s\left(\lambda + (1 - \lambda)e^{-\tau s}\right) - \lambda\beta\left(1 - e^{-\tau s}\right)} \tag{16}$$

The transfer function $H(s)$ indicates the additional dynamics between the virtual control ν and the state derivative $\dot{x}$ introduced by the model mismatch λ and consideration of F. The stability condition for Eq. (16) will be discussed and proven in detail in Proposition 1 later in this Note. The robustness of scalar INDI controlled systems will now be explained by testing the responses of $H(s)$ as follows, in both time domain and frequency domain.

First, denote the time response of $H(s)$ to a step input as $h(t)$. According to the final value theorem, the steady-state response of $h(t)$ to a step input is calculated as

$$\begin{aligned}
\lim_{t \to \infty} h(t) = \lim_{s \to 0} s\left[H(s)\frac{1}{s}\right] &= \lim_{s \to 0} \frac{s}{s\left(\lambda + (1 - \lambda)e^{-\tau s}\right) - \lambda\beta\left(1 - e^{-\tau s}\right)} \\
&= \lim_{s \to 0} \frac{1}{\lambda + (1 - \lambda)e^{-\tau s} + s\tau(\lambda - 1)e^{-\tau s} - \tau\lambda\beta e^{-\tau s}} \\
&= \frac{1}{1 - \tau\lambda\beta} \approx 1
\end{aligned} \tag{17}$$

in which, as the limit of $H(s)$ is an indeterminate form of $\frac{0}{0}$, L'Hôpital's rule is applied in the second line to calculate the derivative of both the numerator and denominator.

The approximate equality of Eq. (17) uses the assumption that $|\tau\lambda\beta| \ll 1$, which is valid when choosing a very small τ. This requirement is actually consistent with the fact demonstrated by Eq. (6) that when the sample time (i.e. τ) becomes infinitesimal, the contribution of F (β in the scalar case) to the system approaches zero. Hence, Eq. (17) verifies that the way INDI is robust to F is that any error induced by its influence can be reduced to be negligible with a designed sampling rate. Besides, Eq. (17) also indicates that its step response is robust to the model uncertainty level λ. Indeed, thanks to the fact that $\lim_{s \to 0}(\lambda + (1 - \lambda)e^{-\tau s}) = 1$, Eq. (17) guarantees that for $\lambda \neq 1$, the steady-state response of $H(s)$ to a step input converge to 1, under the stability condition given later in Proposition 1.

In addition, to investigate the robustness of $H(s)$ towards sinusoidal signals, we need to discuss the frequency response feature of Eq. (16). As $H(s)$ is an irrational transfer function with transport delay $e^{-\tau s}$ factors in its denominator, it is not straightforward to summarize its frequency-response behavior. Thus we introduce a first-order Padé approximation of $H(s)$, i.e. $H^*(s)$, to demonstrate its properties:
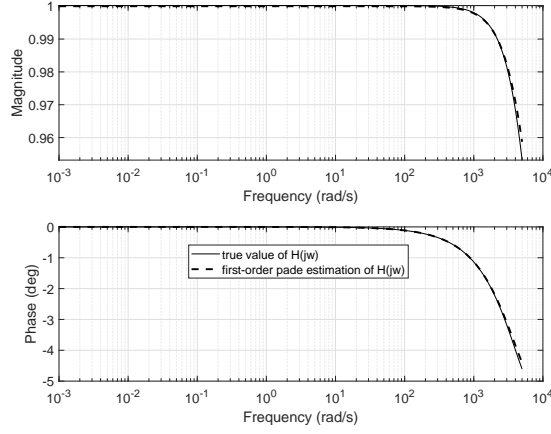
Fig. 2 Frequency response of $H(s)$ and its estimation $H^*(s)$ ($\beta = 1, \lambda = 1.1, \tau = 0.0002$)

$$H(s) \approx H^*(s) = \frac{\tau s + 2}{(2\lambda - 1)\tau s + 2 - 2\lambda\beta\tau} \approx \frac{\tau s + 2}{(2\lambda - 1)\tau s + 2} \tag{18}$$

which is obtained by replacing $e^{-\tau s}$ by its first-order Padé approximation $e^{-\tau s} \approx \frac{2 - \tau s}{2 + \tau s}$, and again using the assumption $|\tau\lambda\beta| \ll 1$ with a small τ.

Thus, $H^*(s)$ is a unit-gain lead- or lag compensator with a zero at $\left(-\frac{2}{\tau}, 0\right)$ and a pole at $\left(-\frac{2}{(2\lambda-1)\tau}, 0\right)$. When $0.5 < \lambda < 1$, $H^*(s)$ is a lead compensator; if $\lambda > 1$, $H^*(s)$ is a lag compensator; in case $\lambda = 1$ (no model mismatch), it is a unit gain. As a lead- or lag compensator, $H^*(s)$ has two corner frequencies, i.e. $\frac{2}{\tau}$ for its numerator and $\frac{2}{(2\lambda-1)\tau}$ for its denominator. If we consider a frequency range that is significantly lower than both corner frequencies of $H^*(s)$, the response of $H^*(s)$ is approximately a unit gain with negligible phase shift, i.e.,

$$H^*(j\omega) \approx 1, \text{if } \omega \ll \min\left(\frac{2}{\tau}, \frac{2}{(2\lambda - 1)\tau}\right) \tag{19}$$

In fact, considering the typical sampling frequency of INDI controller of a few thousand Hz, the corner frequencies of $H^*(s)$, i.e., $\frac{2}{\tau}$ and $\frac{2}{(2\lambda-1)\tau}$, are in the order of magnitude of a few thousand rad/s. Thus the condition of Eq. (19) is generally easily met by the practical input of $\nu(t)$ if it is a sinusoidal signal. As an example, Fig. 2 shows the frequency response of $H(s)$ and its estimation $H^*(s)$ when $\beta = 1$, $\lambda = 1.1$ (thus $\hat{G}$ is 10% larger than G), with a sampling rate of 5000 Hz ($\tau = 0.0002$). From Fig. 2 it is clear that for a frequency lower than 1000 rad/s, the magnitude is approximately equal to 1 and the phase shift is less than 1 degree. It is also clear in Fig. 2 that in this frequency range, $H^*(s)$ is an accurate estimation of $H(s)$. Indeed, the Padé approximation is most accurate at low frequencies.

The above analysis of Fig. 2 can clearly explain the robustness of INDI. With large parameter offset (i.e., $\lambda \neq 1$), the frequency response of $H(s)$ is approximately equal to a unit gain in a relatively low frequency range compared to the sampling frequency of the controller. Eq. 8 still holds if the system input is within this frequency range. This will not

be achieved by NDI controllers and is where the proposed INDI controller improved on. The requirement that the input signal frequency is at least an order of magnitude lower than the controller sampling frequency is a solid assumption for aircraft control, considering that the controller (i.e., INDI) can be sampled at hundreds or even thousands Hertz.

So far the robustness of INDI control method to model uncertainties in G is verified for a scalar system without actuator dynamics. Now the stability conditions for the scalar system in Eq. (16) are given by the following proposition.

Proposition 1: *Assume that $\lambda > 0.5$ then the following assertions hold:*

1) *The system in Eq. (16) is stable and independent of delay if $\beta \leq 0$.*

2) *The system in Eq. (16) is delay-dependent stable if $\beta > 0$, the corresponding time-delay margin is: $\tau^* = \frac{1}{\lambda\beta}$. Furthermore, the system is unstable for any $\tau > \tau^*$.*

Proof: First, as discussed in the Section III.A, the necessary condition for the stability of Eq. (16) (which is the SISO case of Eq. (12)) is that its neutral part given in Eq. (14) is stable. Applying the definition $\lambda = \hat{G}G^{-1}$, we can easily obtain the characteristic equation of Eq. (14) as:

$$\lambda + (1 - \lambda)\, e^{-\tau s} = 0 \tag{20}$$

It is clear that if and only if $\lambda > 0.5$, Eq. (20) has all roots located in the closed left-half plane. Thus $\lambda > 0.5$ is the necessary condition for the stability for Eq. (16).

With this precondition, the characteristic equation associated with Eq. (16) can be expressed in a standard form [25]:

$$s\,(1 - de^{-\tau s}) + a + be^{-\tau s} = 0 \tag{21}$$

where $d = 1 - \lambda^{-1}$, $a = -\beta$ and $b = \beta$. The first part of Proposition 1 can be directly proven following the same steps as the proof provided in Ref. [25] for its Proposition 3.17. The second part of Proposition 1 can be derived with standard D-decomposition (also called D-partitions) method discussed in [24–26]. For a quick calculation, Silviu [25] derived the time-delay margin of Eq. (21) in Eq (3.83). Directly substituting $a = -\beta$ and $b = \beta$ into this equation gives us a form of $0/0$, thus one can calculate its limit as $a \to -\beta$ and $b \to \beta$. As the result, for the studied system, the time-delay margin can be calculated as

$$\tau^* = \lim_{a \to -\beta} \sqrt{\frac{1 - d^2}{b^2 - a^2}} \arctan \frac{bd - a}{\sqrt{(b^2 - a^2)(1 - d^2)}} \Bigg|_{d=1-\lambda^{-1},b=\beta} = \frac{1}{\lambda\beta} \tag{22}$$

which defines the time-delay margin for stability. □

Proposition 1 shows that for a stable local linear system in Eq. (4), the INDI controller is stable if and only if $\lambda > 0.5$ holds. Note this single condition gives both upper bound and lower bound for the gain $\hat{G}^{-1}$ used in the INDI control

law, i.e. $0 < \hat{G}^{-1} < 2G^{-1}$ (if $G > 0$). When the local linear system is unstable (when $\beta > 0$), the stability condition is $\tau < 1/\lambda\beta$. Please note that for its derivation it is not necessary to assume that λ and β are independent parameters. This turns out to be an inherently satisfied condition for INDI since $\tau \ll 1/\lambda\beta$ is a requirement for performance, as shown in Eq. (17). Indeed, in practical applications, the sample time of INDI is chosen far below the time-delay margin to guarantee performance. Also, a quantified stability condition for the control effectiveness offset is given by $0.5 < \lambda < 1/\tau\beta$ (when $\beta > 0$). It will be derived in Sec. IV that the existence of actuator dynamics will in reality further relax this lower bound for an appropriate choice of τ, which further enhances the robustness of INDI.

C. Multiple-Input-Multiple-Output (MIMO) Systems

Similar to the SISO case, the stability conditions for a general INDI controlled multidimensional system in Eq. (12) can be obtained by investigating the associated characteristic quasi-polynomial $p(s, e^{-\tau s})$. Using the stability conditions, the parameter uncertainty bound regarding the mismatch of the control effectiveness matrix G can be given in an explicit form with the following Proposition.

Proposition 2: *Assume that the square matrix $\hat{G}G^{-1}$ is diagonalizable and has non-zero eigenvalues denoted by λ_i. Then the necessary condition for the time-delay system in Eq. (11) to be stable is that the real part of all its eigenvalues satisfies $Re(\lambda_i) > 0.5$.*

Proof: As discussed before, the necessary condition for the NFDE to be stable is that their neutral parts are stable [21]. For the studied system in Eq. (11), this requires that Eq. (14) is stable. Assuming that $\hat{G}$ and G are invertible, Eq. (14) can be written as

$$\dot{x}(t) + \left[G\hat{G}^{-1} - I\right]\dot{x}(t - \tau) = 0 \tag{23}$$

Denoting $\rho(\cdot)$ as the spectral radius of a matrix (which is the largest absolute value of its eigenvalues), the sufficient and necessary condition for Eq. (23) to be stable is that [23]

$$\rho\left(G\hat{G}^{-1} - I\right) = \max\{|\lambda_1^{-1} - 1|, \ldots, |\lambda_n^{-1} - 1|\} < 1 \tag{24}$$

which requires that $|\lambda_i^{-1} - 1| < 1$ holds for every λ_i. Indeed, as λ_i are defined as the eigenvalues of $\hat{G}G^{-1}$, $\lambda_i^{-1} - 1$ are thus the eigenvalues of the matrix $G\hat{G}^{-1} - I$. Assuming that $\lambda_i = \sigma_i + \omega_i j$, we obtain

$$|\lambda_i^{-1} - 1| = \left|\frac{1}{\sigma_i + \omega_i j} - 1\right| = \sqrt{\frac{\left(\sigma_i^2 + \omega_i^2\right)^2 + (1 - 2\sigma_i)\left(\sigma_i^2 + \omega_i^2\right)}{\left(\sigma_i^2 + \omega_i^2\right)^2}} \tag{25}$$

It is apparent from Eq. (25) that $|\lambda_i^{-1} - 1| < 1$ if and only if $\sigma_i > 0.5$, thus, $Re(\lambda_i) > 0.5$ is the necessary condition for stability. $\qquad\square$

Proposition 2 extends the uncertainty bound for G to MIMO systems. The eigenvalues λ_i actually indicate the level

of mismatch between the matrices $\hat{G}$ and G, equivalent to λ in Proposition 1. When $\hat{G} = G$, $\lambda_i = 1$ and no offset exists for G. When the model mismatch in $\hat{G}$ is within the margin given by Proposition 2, the dynamics of the controlled system can be analyzed as follows.

Assuming that the sampling period of the INDI controller is chosen significantly smaller than the time-delay margin, such that Eq. (6) holds and the F related terms in Eqs. (10)-(11) are decreased to be negligible. Thus, the INDI controlled system dynamics in Eq. (11) are dominated by its neutral part:

$$\hat{G}G^{-1}\dot{x}(t) + \left[I - \hat{G}G^{-1}\right]\dot{x}(t - \tau) = \nu(t) \tag{26}$$

Diagonalizing the matrix $\hat{G}G^{-1}$ through the following eigenvalue decomposition

$$\hat{G}G^{-1} = M\Lambda M^{-1} \tag{27}$$

and taking the corresponding linear transformation

$$\chi = M^{-1}x, \; \upsilon = M^{-1}\nu \tag{28}$$

Equation (26) is diagonalized as

$$\Lambda\dot{\chi}(t) + (I - \Lambda)\dot{\chi}(t - \tau) = \upsilon(t) \tag{29}$$

which is decoupled into n scalar differential equations:

$$\lambda_i\dot{\chi}_i(t) + (1 - \lambda_i)\dot{\chi}_i(t - \tau) = \upsilon_i(t), \; i = 1\ldots n \tag{30}$$

As a result, the transfer function between the transformed virtual control υ and χ can be given as

$$\frac{s\chi_i(s)}{\upsilon_i(s)} = H_i(s) = \frac{1}{\lambda_i + (1 - \lambda_i)e^{-\tau s}}, \; i = 1\ldots n \tag{31}$$

Equation (31) indicates that each eigenvalue of $\hat{G}G^{-1}$ parameterizes a single SISO time-delay system $H_i(s)$. The transfer function $H_i(s)$ is in fact identical to $H(s)$ in Eq. (16) when the β-related term is neglected with an infinitesimal τ. Thus $H_i(s)$ has the same robust features as $H(s)$ in Eq. (18) as discussed in Section III.B, which can be approximated by a lead/lag compensator, with its poles decided by the value of λ_i.

It is clear that the decoupling technique and linear transformation introduced in Eq. (27) to (31) enables simplified stability and robustness analysis. For a multi-dimensional system, the characteristic equation of Eq. (26) features a high dimensional quasi-polynomial that is difficult to analyze. With the linear transformation, the system is decoupled into

11

n SISO systems, each with low-order quasi-polynomials parameterized by the quantified model mismatch indicator λ_i. This advantage is more obvious when analyzing MIMO systems considering actuator dynamics, which will be discussed in more detail in the next section.

IV. Stability conditions in existence of actuator dynamics

The stability conditions given in Propositions 1 and 2 reveal the theoretical limits on control effectiveness matrix mismatches to be $\lambda > 0.5$ or $Re\,(\lambda_i) > 0.5$ without consideration of any actuator dynamics. Nevertheless, in recent high-fidelity simulations and experiments of INDI-based flight control systems (e.g., [9]), for which real-life actuator dynamics were present, it was demonstrated that even when $\lambda = 0.1$ (when the control effectiveness of the simulation model is increased by 1000%), the control system is still stable, despite suffering from oscillations. In this section, it will be demonstrated that the presence of practical (so not infinitely fast) actuators will actually relax the parameter bound of INDI with respect to λ or λ_i, with a possible compromise in performance.

A. Open-loop stability

In real-world applications of INDI, as shown in Fig. 1, actuator dynamics $A\,(s)$ play a key role in the control system. Consider the actuator dynamics $A\,(s)$ in Fig. 1 as a designed servo-system, the dynamics of which can be described by a low-order system model. The control input after the actuator can be described in the *s*-domain as:

$$\mathcal{U}\,(s) = A\,(s) \left[e^{-\tau s}\mathcal{U}\,(s) + G^{-1}\,(\mathcal{V}\,(s) - e^{-\tau s}s\mathrm{X}\,(s)) \right] \tag{32}$$

where $\mathcal{U}\,(s)$, $\mathrm{X}\,(s)$ and $\mathcal{V}\,(s)$ are the Laplace transform of $u\,(t)$, $x\,(t)$ and $v\,(t)$.

Again, we assume that the chosen sampling period of INDI is significantly smaller than the calculated time-delay margin, such that the F-related term in Eq. (10) is negligible. Thus, the Laplace transform of Eq. (10) can be written as

$$s\mathrm{X}\,(s) = se^{-\tau s}\mathrm{X}\,(s) + G\left[\mathcal{U}\,(s) - e^{-\tau s}\mathcal{U}\,(s)\right] \tag{33}$$

Substituting Eq. (32) into Eq. (33), the dynamics of INDI controlled closed-loop system are given by:

$$\left[\hat{G}G^{-1} + A\,(s)\,e^{-\tau s}\left(I - \hat{G}G^{-1} \right) \right] s\mathrm{X}\,(s) = A\,(s)\,\mathcal{V}\,(s) \tag{34}$$

Considering the same eigenvalue decomposition and linear transformation in Eqs. (27) and (28) for Eq. (34) we have

$$[\Lambda + A\,(s)\,e^{-\tau s}\,(I - \Lambda)]\,s\chi\,(s) = A\,(s)\,v\,(s) \tag{35}$$

which is decoupled into *n* scalar systems. Note that $A\,(s) = \mathrm{diag}\,(A_1\,(s)\,, A_2\,(s)\,, ..., A_n\,(s))$, thus the transfer functions
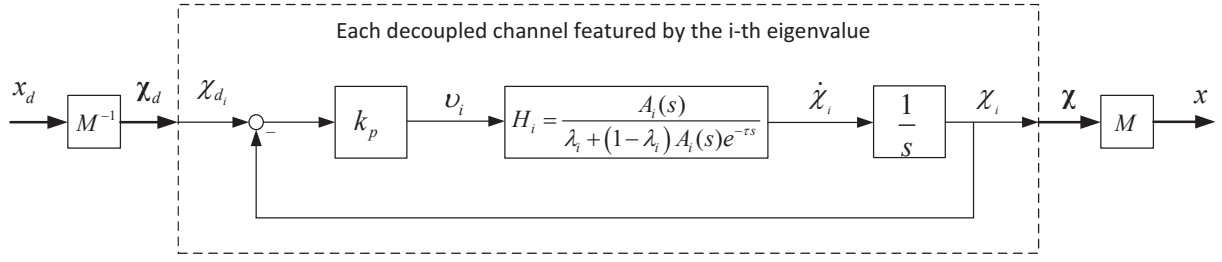
Fig. 3   INDI-controlled MIMO system decoupled into n parallel SISO systems ($i = 1, 2, ..., n$)

between the virtual controls and the state derivatives are:

$$\frac{s\chi_i(s)}{\upsilon_i(s)} = H_i(s) = \frac{A_i(s)}{\lambda_i + (1 - \lambda_i) A_i(s) e^{-\tau s}}, \quad i = 1 \ldots n \tag{36}$$

This means that the practical INDI-controlled system can be analyzed with an equivalent decoupled system with n parallel channels, as demonstrated by Fig. 3. The dynamics of each individual channel are defined by the value of λ_i.

Thus, Eq. (36) describes the additional dynamics brought to the INDI-controlled single integrator in Eq. (8), with time-delay effects, control effectiveness uncertainties, and actuator dynamics taken into consideration. When no model mismatch exists for G and $\lambda_i = 1$, the additional dynamics are equal to the actuator dynamics, i.e., $H_i(s) = A_i(s)$. When $\lambda_i \neq 1$, the fact that $\lim_{s \to 0} s \left[H(s) \frac{1}{s}\right] = 1$ still holds if $A_i(s)$ itself is stable. This confirms the robustness against $\lambda_i \neq 1$ of INDI, as the state derivative will always converge to the virtual control for a step input. The existence of model uncertainties in G helps to reshape the equivalent actuator dynamics H_i in INDI as an explicit function of λ_i. Thus, the stability conditions for the value of λ_i is now of concern.

The stability of Eq. (36) can be examined by investigating the root locations of its characteristic equation. In this Note, for simplicity, the actuator dynamics are considered as a first-order system: $A_i(s) = 1/(\tau_a s + 1)$, as is commonly assumed in flight control systems [27]. Hence, Eq. (36) becomes

$$H_i(s) = \frac{1}{(\tau_a s + 1) \lambda_i + (1 - \lambda_i) e^{-\tau s}} \tag{37}$$

which represents a *retarded* functional differential equation, instead of a neutral FDE, as the term $se^{-\tau s}$ no longer exists. As a single time-delay system, the direct analytical method [18] can be used to find the stability conditions for Eq. (37). For simplicity, considering λ_i to be real numbers, the characteristic equation of Eq. (37) can be written in a well-known form:

$$s + a + be^{-\tau s} = 0 \tag{38}$$

where $a = \tau_a^{-1}$ and $b = \tau_a^{-1}\left(\lambda_i^{-1} - 1\right)$. According to Ref. [25], when $a > |b|$, which means $\lambda_i \geq 0.5$, Eq. (38) is stable

independent of the delay. When $\lambda_i < 0.5$, it is stable dependent of the time delay and the delay margin is given by [18, 25]

$$\tau \le \tau^* = \frac{\pi - \cos^{-1}\left(\frac{a}{b}\right)}{\sqrt{b^2 - a^2}} = \tau_a \frac{\pi - \cos^{-1}\left(\frac{1}{\lambda_i^{-1} - 1}\right)}{\sqrt{\lambda_i^{-1}\left(\lambda_i^{-1} - 2\right)}} = \tau_a h\left(\lambda_i\right) \tag{39}$$

Equation (39) shows, for the first time, that the time-delay margin is proportional to the time constant of the actuator, at a ratio being a function of λ_i, i.e., $h\left(\lambda_i\right)$. It also means that when the actuator dynamics are considered, $\lambda_i > 0.5$ is a sufficient condition for stability of the equivalent retarded system, instead of necessary condition as in neutral cases when actuator dynamics are assumed to be infinitely fast. The stability condition for λ_i is in fact given by Eq. (39) as:

$$\lambda^* = h^{-1}\left(\frac{\tau}{\tau_a}\right) = h^{-1}\left(r\right) \tag{40}$$

where r is the ratio between τ and τ_a and $h^{-1}\left(\cdot\right)$ is the inverse function of $h\left(\cdot\right)$ defined in Eq. (39). As the analytical expression of this inverse function is difficult to obtain, it is common to apply Padé estimation for the delay $e^{-\tau s}$. Rational approximations of Eq. (37) with the first- and second-order Padé estimations of $e^{-\tau s}$ give

$$H_1^*(s) = \frac{\tau s + 2}{\lambda_i \tau_a \tau s^2 + (2\lambda_i \tau_a + 2\lambda_i \tau - \tau)\,s + 2} \tag{41}$$

and

$$H_2^*(s) = \frac{\tau^2 s^2 + 6\tau s + 12}{\lambda_i \tau_a \tau^2 s^3 + \left(\tau^2 + 6\lambda_i \tau_a \tau\right) s^2 + (12\lambda_i \tau + 12\lambda_i \tau_a - 6\tau)\,s + 12} \tag{42}$$

This means that the time-delay dynamics introduced by the INDI controller can be approximated by a second or third-order system, instead of the lead/lag compensator found when actuator dynamics are neglected. The equivalent poles of the approximated systems are decided by the mismatch indicator λ_i, the time constant of the actuator τ_a and the INDI controller sampling time τ. According to Routh's Stability Criterion, the stability of the equivalent systems $H_1^*(s)$ and $H_2^*(s)$ requires the boundary of λ_i to be

$$\lambda_i > \begin{cases} \lambda_1^* = \frac{1}{2}\left(\frac{\tau}{\tau_a + \tau}\right) = \frac{1}{2}\left(\frac{r}{1+r}\right), \\ \lambda_2^* = \frac{3\tau_a \tau - \tau^2 + \tau\sqrt{\tau^2 + 21\tau_a^2 + 6\tau_a \tau}}{12\tau_a \tau + 12\tau_a^2} = \frac{3r - r^2 + r\sqrt{r^2 + 6r + 21}}{12r + 12} \end{cases} \tag{43}$$

where λ_1^* and λ_2^* are the first and second-order estimates of the uncertainty bound λ^* for the model mismatch level in G, respectively. When the actuator dynamics are considered infinitely fast such that $\tau_a = 0$, we have $\lambda_1^* = \lambda_2^* = 0.5$, which is consistent with the stability condition given in Proposition 1 and 2.

Figure 4 plots the numerically calculated stability condition λ^* from Eqs. (40) and (39), as well as its first and second-order estimates, λ_1^* and λ_2^* in Eq. (43). It is clear that the second-order estimation λ_2^* already results in good
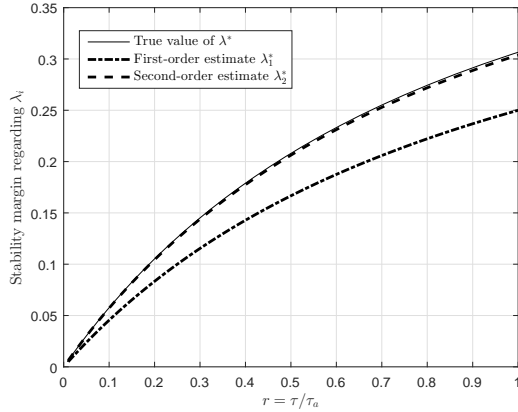
Fig. 4 Open-loop stability region in terms of λ_i given by Eq. (40), and its first- and second-order approximations.
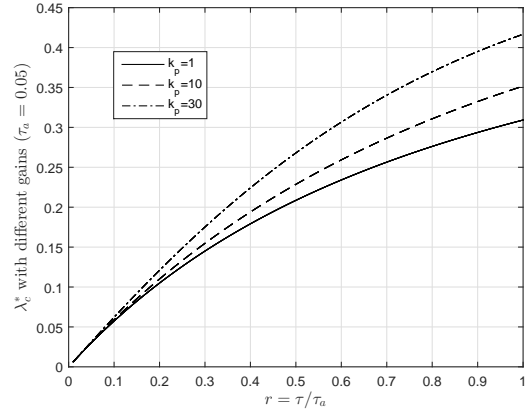
Fig. 5 The curve of the closed-loop stability condition defined by λ_c^* with different values of k_p.

accuracy. Apparently, given a particular actuator time constant τ_a, a higher controller sampling rate (smaller r) guarantees a lower boundary of λ_i, which indicates an improved robustness. Consider a typical bandwidth of a flight control actuator to be 20 rad/s and the sampling rate of the INDI controller to be 100 Hz ($r = 0.2$), the parameter uncertainty bound is $\lambda^* \approx 0.1$, which is significantly relaxed compared to the case with neglected actuator dynamics, which was 0.5. It should be noted that the uncertainty bound derived in this section represents the open-loop stability condition for the equivalent transfer functions $H_i(s)$, as shown in Fig. 3. When INDI is applied to higher-order systems, such as typical robotic systems, feedforward terms are of preference to be added to υ_i, instead of only the feedback term as demonstrated in Fig. 3 for first-order systems. Thus, in the general case, the open-loop stability of $H_i(s)$ described in this section is a necessary condition for the stability of the entire system. In the following section, the stability conditions for the closed-loop system will be discussed.

B. Closed-loop stability

With the block diagrams of the decoupled channels given in Fig. 3, it is convenient to determine the stability condition for the closed-loop system. Again, assuming the actuator dynamics to be first-order systems $A(s) = 1/(\tau_a s + 1)$, the transfer function from χ_{d_i} to χ_i in Fig. 3 is easily calculated as

$$T_{\chi_{d_i} \to \chi_i} = \frac{k_p H_i(s)}{s + k_p H_i(s)} = \frac{k_p}{\tau_a \lambda_i s^2 + \lambda_i s + (1 - \lambda_i) s e^{-\tau s} + k_p} \tag{44}$$

The corresponding characteristic equation features a second-order time-delay system:

$$\tau_a \lambda_i s^2 + \lambda_i s + (1 - \lambda_i) s e^{-\tau s} + k_p = 0 \tag{45}$$

15

Notable here that when the actuator dynamics are negligible, $\tau_a = 0$ and Eq. (45) still represents a neutral system. The necessary condition for its stability is still $Re\,(\lambda_i) > 0.5$, equivalent to the open-loop condition given by Proposition 2.

When the actuator dynamics are considered, however, Eq (45) represents a second-order RFDE, the stability of which is not only decided by λ_i, τ and τ_a, but also by the linear controller gain k_p. The time-delay margin and stability of Eq. (45) can still be analytically calculated with the direct method given in Ref. [18], but a closed-form solution is cumbersome to achieve. Thus, for engineering practice, a rational approximation of the closed-loop transfer function in Eq. (44) with the second-order Padé approximation of $e^{-\tau s}$ gives

$$T^*_{\chi_{d_i} \to \chi_i} = \frac{\tau^2 s^2 + 6\tau s + 12}{\lambda_i \tau_a \tau^2 s^4 + \left(\tau^2 + 6\lambda_i \tau_a \tau\right) s^3 + \left(12\lambda_i \tau + 12\lambda_i \tau_a - 6\tau + \tau^2 k_p\right) s^2 + \left(12 + 6\tau k_p\right) s + 12 k_p} \tag{46}$$

using Routh's Stability Criterion, the stability condition in terms of λ_i can be given as:

$$\lambda_i > \lambda_c^* = \frac{6\tau_a \tau - 2\tau^2 + 5\tau^2 \tau_a k_p - \tau^3 k_p + \tau \sqrt{\left(\tau k_p + 2\right)^2 \left(\tau^2 + 6\tau_a \tau + 21\tau_a^2 - 2\tau^2 \tau_a k_p\right)}}{12 \left(\tau^2 \tau_a k_p + 2\tau \tau_a + \tau_a^2\right)} \tag{47}$$

It is clear from Eq. (47) that when k_p approaches 0, the estimated closed-loop stability condition coincides with the open-loop case, i.e., $\lambda_c^* = \lambda_2^*$. The influence of k_p to the closed-loop system stability increases with the value of k_p. Figure 5 plots the calculated λ_c^* against the time delay when $\tau_a = 0.05$, with different values of k_p. It is clear that the robustness against λ_i decreases when k_p increases. Equation (47) can thus also act as a guideline for choosing suitable linear controller gains for INDI controlled systems.

With the derived time-delay dynamics $H_i\,(s)$ in Eq. (36) and its approximation in Eqs. (41) and (42), it is easy to explain why, for an INDI controller with actuator dynamics, a particular model mismatch in $\hat{G}$ may give better performance than using the true value of G.

C. Optimal control effectiveness matrix for INDI

Consider the first-order approximation of H_1^* in Eq. (41). Once the actuator time constant τ_a and the controller sampling time τ are set, the locations of the poles of H_1^* will move as λ_i changes. Figure 6 demonstrates the root locations of the characteristic equation of the open-loop transfer function H_1^* with λ_i decreasing from $+\infty$ to the uncertainty bound λ_1^*. When λ_i approaches $+\infty$, the two poles are located on the negative real axis and will converge to the origin and $(-2\,(\tau_a + \tau)\,/\tau_a \tau, 0)$. As λ_i decreases, the two poles move toward each other. When $\lambda_i = 1$, the poles move to $(-1/\tau_a, 0)$ and $(-2/\tau, 0)$. As the left pole is far away from the imaginary axis, and cancelled by the zero of H_1^* at $(-2/\tau, 0)$, the transfer function is equal to $A_i\,(s)$. when $\lambda_i > 1$, the dominant pole is even closer to the imaginary axis, the bandwidth of H_1^* is slower than $A_i\,(s)$. Thus, the model mismatch in $\hat{G}$ caused by an *overestimation* of G will decrease the control system performance by slowing down the inner-loop dynamics.
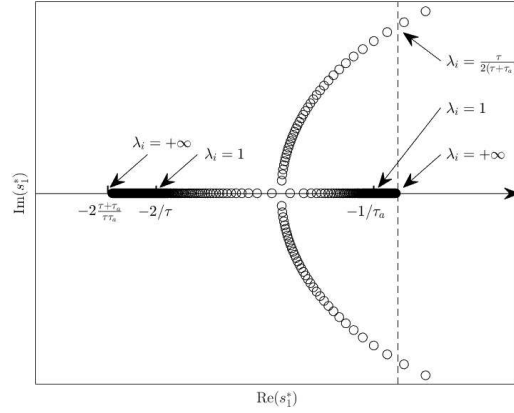
Fig. 6 The poles of H_1^* as λ_i changes

When λ_i decreases to be less than 1, the poles continue moving toward each other with the dominant pole moving away from the imaginary axis. As a result, the bandwidth of the system is actually increased, which results in a performance improvement. As λ_i continues to decrease, the poles meet at the negative real axis and split into two complex conjugate pairs. When $\lambda_i = \lambda_1^*$, the root trajectories cross the imaginary axis and the system becomes unstable. Apparently, a good choice of *underestimated G* (i.e. $\lambda_i < 1$) results in better dynamic characteristics for H_1^*. The transient response of the resulting transfer function $H_i(s)$ in Eq. (36) has better performance than the actuator dynamics $A_i(s)$, to which $H_i(s)$ is equal when $\lambda_i = 1$. Note that this optimization is illustrated only for the inner-loop INDI controller, a global optimization needs to consider the outer-loops, for instance, the feedback loop for calculating $\boldsymbol{v}$.

For INDI control systems, $\hat{\boldsymbol{G}}$ is selected as the best available estimation of the true $\boldsymbol{G}$. Particularly for flight control systems, one way to estimate $\boldsymbol{G}$ is directly calculating it using the corresponding nominal aircraft design parameters (i.e. nominal inertial matrix $\hat{\boldsymbol{J}}$, wing surface area $\hat{S}$, control derivatives $\hat{C}_{l_{\delta_a}}$, etc.) in nominal flight condition (see later in Eq. (51)). Alternatively, another intuitive way to obtain the estimation of $\boldsymbol{G}$ is using a proper offline aerodynamic model identification method in nominal flight condition. Note that INDI does not require an online model identification system to obtain the real-time true value $\boldsymbol{G}$ (which traditional NDI approach usually does).

V. Simulation Validation

In this section, the stability condition with respect to model mismatch and time-delay, which was derived in this Note, will be validated by numerical simulations of an INDI angular-rate controller for a fixed-wing aircraft model.

The aircraft model used in this Note is a 6-DOF nonlinear model of a fixed-wing business jet, the Cessna Citation 500. The model is developed in MATLAB/Simulink, using parameters from the Delft University Aircraft Simulation Model and Analysis Tool (DASMAT) [28]. Some of the key parameters of the aircraft model is shown in Table 1. As the detailed angular-rate controller based on INDI for flight control systems has been extensively discussed in various

17

studies [4, 6, 9], it will only be briefly summarized here. The translational and rotational dynamic equations of a rigid-body aircraft are given by

$$\dot{V} = -\omega \times V + m^{-1}(F_a + F_T) + g, \tag{48}$$

$$\dot{\omega} = J^{-1}(M_a - \omega \times J\omega) + J^{-1}M_{c_\delta}\delta \tag{49}$$

where $V = [u, v, w]^T$ is the vector of translational velocities, $\omega = [p, q, r]^T$ is the angular rate vector (roll, pitch, and yaw) along the axes of the body reference frame, and $\delta = [\delta_a, \delta_e, \delta_r]^T$ is the vector of control surface deflections. F_a and F_T represents the aerodynamic and propulsion forces. M_a is the vector of moments generated by the aerodynamics of the airframe and M_{c_δ} the vector of moments generated by the deflections of control surfaces. J is the inertial matrix, m the mass and g the gravity vector projected in the body reference frame, M_{c_δ} is given by

$$M_{c_\delta} = \bar{q}S \begin{bmatrix} bC_{l_{\delta_a}} & 0 & bC_{l_{\delta_r}} \\ 0 & \bar{c}C_{m_{\delta_e}} & 0 \\ bC_{n_{\delta_a}} & 0 & bC_{n_{\delta_r}} \end{bmatrix} \tag{50}$$

where $\bar{q}$ is the dynamic pressure, S the wing surface area, b the wing span and $\bar{c}$ the mean aerodynamic chord.

Currently, for flight control systems, INDI is most commonly applied as the inner-loop angular-rate controller. Considering the rotational dynamics in Eq. (49), with the states $x = \omega$ and control inputs $u = \delta$, and by applying the INDI control method given in Eq. (3) to (9), the angular-rate control law is given by [4]

$$u(t) = \delta(t-\tau) + \underbrace{\hat{M}_{c_\delta}^{-1}\hat{J}}_{\hat{G}^{-1}}(v(t) - \dot{\omega}(t-\tau)) \tag{51}$$

where the delayed measurements of the control surface deflections $\delta(t-\tau)$ and the angular accelerations $\dot{\omega}(t-\tau)$ are assumed to be accurate and noise-free. Neglecting the small terms as in Eq. (3), the system is linearized to $\dot{\omega} = v$. Given a required angular velocity ω_d from the outer-loop, the virtual control can be simply chosen to be $v = K_p(\omega_d - \omega)$. For all simulated conditions, the simulation frequency is 10 kHz, while the INDI controller is sampled at 100 Hz. The control surfaces (actuators) are modeled as first-order systems defined by the transfer function $A_i(s) = 1/(\tau_a s + 1)$, and the deflection limits are set to ±30° for δ_a, δ_e and δ_r, respectively.

In order to validate the proposed stability conditions, doublet inputs are designed for the pitch rate with deliberately introduced model mismatches in the control effectiveness $\hat{G}$ implemented in Eq. (51). First, the time constant τ_a for the actuator models is set to 0, neglecting all actuator dynamics. The mean aerodynamic chord $\bar{c}$ used for the controller is offset from its true value with three levels of underestimation, such that the minimum eigenvalue of $\hat{G}^{-1}G$, i.e., λ_2, decreases from 1 to 0.49, 0.5 and 0.51, respectively. The corresponding simulation results are given in Fig. 7, and the different phases are shown in different shades of grey. From 0 to 22 seconds (dark grey), the system is

unstable with $\lambda_2 = 0.49 < 0.5$, where the elevators are fully saturated (Fig. 7(a)) and the response of the system shows unstable high-frequency oscillations in the pitch rate (Fig. 7(b)). From 22 to 42 seconds (medium grey), λ_2 is set to 0.5. As clearly shown in the insets in the upper-right windows of Fig. 7, any unstable oscillations decay over time and the controlled system demonstrates marginally stable behaviour. The pitch manoeuvres q are correctly tracked with sustained oscillations. The elevators still demonstrate chattering-like behaviour, but are no longer saturated. After 42 seconds, the stability condition given in Proposition 2 is satisfied with $\lambda_2 = 0.51 > 0.5$, which is consistent with the simulation performance shown in the light-grey area of Fig. 7. The doublet inputs are perfectly tracked with good transient performance, despite the fact that small oscillations are still observed for the actuators at the moment of manoeuvre initiation. These results further validate the stability condition given by Proposition 2, when the actuator dynamics are neglected.

Table 1   Key parameters of the Cessna Citation model

Mass$[kg]$	Wing area$[m^2]$	Mean chord$[m]$	Wingspan$[m]$
4500	25	2	13.325

(a) Deflections of elevators

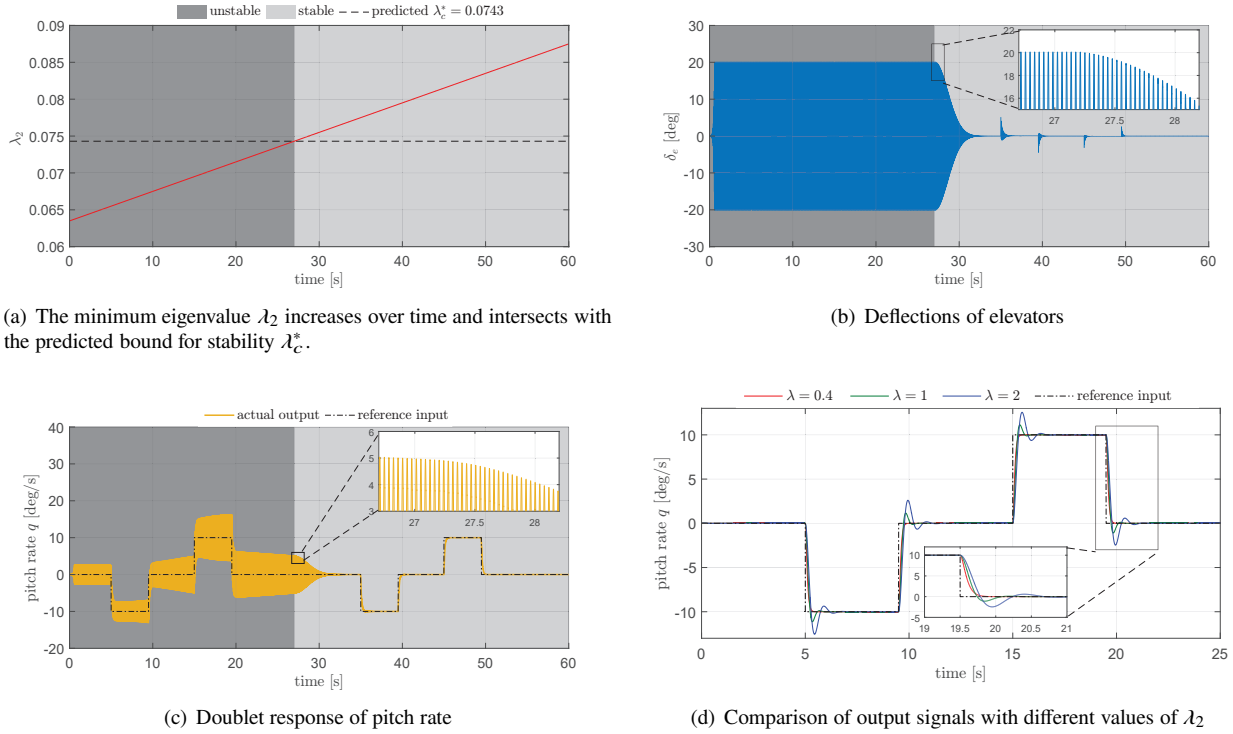(b) Doublet response of pitch rate
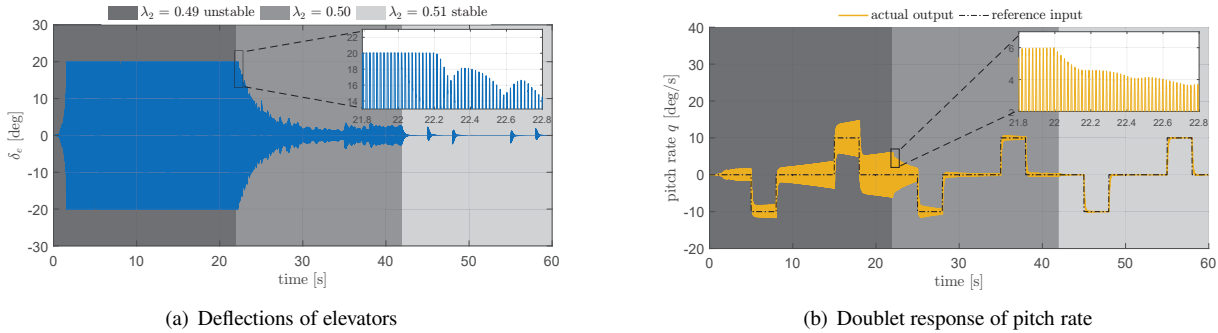
Fig. 7   Simulation results under different levels of parameter mismatch, without actuator dynamics

In order to validate the stability conditions developed for practical cases with finite actuator bandwidths, similar doublet response simulations are performed with the time constant of the elevator $\tau_a = 0.08s$. The linear control gains are chosen to be $\boldsymbol{K}_p = 10\boldsymbol{I}$. As no feedforward term is implemented for the virtual control $\boldsymbol{v}$, only the closed-loop stability condition given in Section IV.B needs to be considered. According to the second-order estimate given by Eq. (47), the estimated bound for stability in terms of λ_i ($i = 2$) is easily calculated as $\lambda_c^* \approx 0.0743$. Thus, in this simulation the mean aerodynamic chord $\bar{c}$ used for the controller in $\hat{\boldsymbol{G}}$ is set to be around 0.065 times its true value at the starting instance, which slowly increases over time. This results in a minimum eigenvalue λ_2 of $\hat{\boldsymbol{G}}^{-1}\boldsymbol{G}$ that is smaller than λ_c^* at the beginning of the simulation, which slowly increases over time, as shown in Fig. 8(a). At around $t = 27$ s, λ_2 intersects with λ_c^* and the controlled system enters the stable region.

The corresponding elevator deflections and tracking performance of the pitch rate are shown in Fig. 8(b) and (c).

When $t < 27$ s, $\lambda_2 < \lambda_c^*$, the pitch-rate response shows unstable oscillations, while the elevators are fully saturated with oscillations of the same pattern. For $t > 27$ s, when the system is within the calculated stable region, the unstable oscillations quickly die out, and the controlled system gives stable tracking performance with good transient responses. This obvious change in system behaviour can be clearly observed in the insets in Fig. 8, when λ_2 intersects with λ_c^*.

(a) The minimum eigenvalue λ_2 increases over time and intersects with the predicted bound for stability λ_c^*.

(b) Deflections of elevators

(c) Doublet response of pitch rate

(d) Comparison of output signals with different values of λ_2

Fig. 8   INDI-controlled system becomes stable as λ_2 increases over time, with actuator dynamics

These results validate the stability condition for λ_i given by Eq. (47), with a finite time constant τ_a of the actuator. It is also noted that the true value of $\bar{c}$ is approximately 1300% of the value assumed for the controller (with λ_2 equal to around 0.07) in this simulation, which validates the fact that the presence of actuator dynamics significantly increases the robustness of the INDI controller against model errors in terms of λ_i. This is one order of magnitude more robust than the margin of the case with (assumed) infinitely fast actuator dynamics, for which $\lambda > 0.5$ should be satisfied.

The simulation are also performed under different levels of constant model mismatches in $\hat{G}$. In Fig. 8(d), the results with λ_2 equal to 0.4 (underestimation), 1 (no mismatch), and 2 (overestimation) are compared. It is shown that the tracking performance at $\lambda_2 = 0.4$ is indeed better than the case of $\lambda_2 = 1$, when the true value of G is used. The case $\lambda_2 = 2$ gives the worst performance. This result validates the analysis given in Section. IV.C, demonstrating that the INDI performance with an underestimated G can outperform the case when the true value of G is used.

VI. Conclusion

This Note addressed some key open theoretical issues for the Incremental Nonlinear Dynamic Inversion (INDI) control technique, regarding its robustness and stability conditions in terms of control effectiveness and sampling period. In this Note, practical actuator dynamics are considered and their influence on INDI's stability and robustness properties is determined explicitly. For stability analysis, an equivalent linear time-delay system with a special robust structure is proposed for general INDI-controlled systems, which enables the robustness to model uncertainties to be quantified explicitly. A quantified parameter uncertainty bound regarding the proposed allowable model mismatch level indicator is derived analytically, together with an accompanying solution for the time-delay margin for a selected controller sampling frequency. A particular (underestimated) control effectiveness matrix $\hat{G}$ with model mismatches for the controller - i.e., different than its true value G - is also found to achieve performance improvement. This allows for future development of online INDI controller sample-time and parameter optimization (and self-tuning) under various disturbances and system failures. Simulation validation was performed on a fully nonlinear model of a fixed-wing aircraft using INDI control. The proposed conditions of uncertainty bound can perfectly predict the stability behaviour of the closed-loop system in the simulations. It is demonstrated that with the proposed "optimal" (underestimated) $\hat{G}$, the control performance is even better than when the perfect control effectiveness G is used. Given as generalizable analytical solutions, the stability conditions proposed in this Note provide much-needed formal guidelines for both analytical and synthesis problems for INDI-controlled systems.

VII. Acknowledgements

References

[1] Enns, D., Bugajski, D., Hendrick, R., and Stein, G., "Dynamic inversion: an evolving methodology for flight control design," *International Journal of Control*, Vol. 59, No. 1, 1994, pp. 71–91. doi:10.1080/00207179408923070.

[2] Saha, D., Valasek, J., Leshikar, C., and Reza, M. M., "Multiple-Timescale Nonlinear Control of Aircraft with Model Uncertainties," *Journal of Guidance, Control, and Dynamics*, Vol. 43, No. 3, 2020, pp. 536–552.

[3] Smith, P., "A simplified approach to nonlinear dynamic inversion based flight control," *23rd Atmospheric Flight Mechanics Conference*, 1998, p. 4461.

[4] Sieberling, S., Chu, Q. P., and Mulder, J. A., "Robust Flight Control Using Incremental Nonlinear Dynamic Inversion and Angular Acceleration Prediction," *Journal of Guidance, Control, and Dynamics*, Vol. 33, No. 6, 2010, pp. 1732–1742.

[5] Huang, Y., Pool, D. M., Stroosma, O., and Chu, Q., "Long-Stroke Hydraulic Robot Motion Control with Incremental Nonlinear Dynamic Inversion," *IEEE/ASME Transactions on Mechatronics*, 2019, pp. 1–1. Dio:10.1109/TMECH.2019.2891358.

[6] Smeur, E. J. J., Chu, Q. P., and de Croon, Guido C., "Adaptive Incremental Nonlinear Dynamic Inversion for Attitude Control of Micro Aerial Vehicles," *Journal of Guidance, Control, and Dynamics*, Vol. 39, No. 3, 2016, pp. 450–461.

[7] Pfeifle, O., and Fichter, W., "Cascaded Incremental Nonlinear Dynamic Inversion for Three-Dimensional Spline-Tracking with Wind Compensation," *Journal of Guidance, Control, and Dynamics*, 2021. doi:https://doi.org/10.2514/1.G005785.

[8] Simplício, P., Pavel, M. D., van Kampen, E., and Chu, Q. P., "An acceleration measurements-based approach for helicopter nonlinear flight control using Incremental Nonlinear Dynamic Inversion," *Control Engineering Practice*, Vol. 21, No. 8, 2013, pp. 1065 – 1077.

[9] Keijzer, T., Looye, G., Chu, Q. P., and Kampen, E.-J. V., "Design and Flight Testing of Incremental Backstepping based Control Laws with Angular Accelerometer Feedback," *AIAA Scitech 2019 Forum, AIAA SciTech Forum*, 2019.

[10] Kim, S., and Bae, J., "Force-Mode Control of Rotary Series Elastic Actuators in a Lower Extremity Exoskeleton Using Model-Inverse Time Delay Control," *IEEE/ASME Transactions on Mechatronics*, Vol. 22, No. 3, 2017, pp. 1392–1400.

[11] Hou, Z., and Xiong, S., "On Model-Free Adaptive Control and Its Stability Analysis," *IEEE Transactions on Automatic Control*, Vol. 64, No. 11, 2019, pp. 4555–4569.

[12] Liu, J., Sun, L., Tan, W., Liu, X., and Li, G., "Finite time observer based incremental nonlinear fault-tolerant flight control," *Aerospace Science and Technology*, Vol. 104, 2020, p. 105986.

[13] Ignatyev, D. I., Shin, H.-S., and Tsourdos, A., "Two-layer adaptive augmentation for incremental backstepping flight control of transport aircraft in uncertain conditions," *Aerospace Science and Technology*, Vol. 105, 2020, p. 106051.

[14] Wang, X., van Kampen, E.-J., and Chu, Q., "Quadrotor fault-tolerant incremental nonsingular terminal sliding mode control," *Aerospace Science and Technology*, Vol. 95, 2019, p. 105514.

[15] Zhou, Y., van Kampen, E.-J., and Chu, Q., "Incremental model based online heuristic dynamic programming for nonlinear adaptive tracking control with partial observability," *Aerospace Science and Technology*, Vol. 105, 2020, p. 106013.

[16] Wang, X., Van Kampen, E.-J., Chu, Q. P., and Lu, P., "Stability Analysis for Incremental Nonlinear Dynamic Inversion Control," *2018 AIAA Guidance, Navigation, and Control Conference*, 2018.

[17] van't Veld, R., Van Kampen, E.-J., and Chu, Q. P., "Stability and Robustness Analysis and Improvements for Incremental Nonlinear Dynamic Inversion Control," *2018 AIAA Guidance, Navigation, and Control Conference*, 2018, p. 1127.

[18] Gu, K., Chen, J., and Kharitonov, V. L., *Stability of time-delay systems*, Springer Science & Business Media, 2003.

[19] Khalil, H. K., *Nonlinear Systems (3rd ed.)*, Prentice Hall, 2002.

[20] Slotine, J.-J. E., Li, W., et al., *Applied nonlinear control*, Vol. 199, Prentice hall Englewood Cliffs, NJ, 1991.

[21] Richard, J.-P., "Time-delay systems: an overview of some recent advances and open problems," *Automatica*, Vol. 39, No. 10, 2003, pp. 1667 – 1694. doi:https://doi.org/10.1016/S0005-1098(03)00167-5.

[22] Gu, K., and Niculescu, S.-I., "Survey on Recent Results in the Stability and Control of Time-Delay Systems*," *Journal of Dynamic Systems, Measurement, and Control*, Vol. 125, No. 2, 2003, pp. 158–165. doi:10.1115/1.1569950.

[23] Fu, P., Niculescu, S.-I., and Chen, J., "Stability of linear neutral time-delay systems: exact conditions via matrix pencil solutions," *Proceedings of the 2005, American Control Conference, 2005.*, 2005, pp. 4259–4264 vol. 6. doi:10.1109/ACC.2005.1470648.

[24] El'sgol'ts, L., and Norkin, S., *Introduction to the Theory and Application of Differential Equations with Deviating Arguments*, Mathematics in Science and Engineering, Academic Press, 1973.

[25] Niculescu, S., *Delay Effects on Stability: A Robust Control Approach*, Lecture Notes in Control and Information Sciences, Springer London, 2003.

[26] Kolmanovskii, V. B., and Nosov, V. R., *Stability of functional differential equations*, Vol. 180, Elsevier, 1986.

[27] Stevens, B., and Lewis, F., *Aircraft Control and Simulation*, Wiley, 1992.

[28] van der Linden, C. A. A. M., "DASMAT-Delft University Aircraft Simulation Model and Analysis Tool: A Matlab/Simulink Environment for Flight Dynamics and Control Analysis," Tech. rep., Delft University of Technology, Faculty of Aerospace Engineering, 1998.